AUTOPHAGY
2021, VOL. 17, NO. 5, 1205–1221
https://doi.org/10.1080/15548627.2020.1753002

Taylor & Francis
Taylor & Francis Group

RESEARCH PAPER

OPEN ACCESS Check for updates

Mitophagy deficiency increases NLRP3 to induce brown fat dysfunction in mice

Myoung Seok Ko[a*], Ji Young Yun[a,b*], In-Jeoung Baek[a], Jung Eun Jang[a,b], Jung Jin Hwang[c], Seung Eun Lee[a,b], Seung-Ho Heo[d], David A. Bader[e], Chul-Ho Lee[f], Jaeseok Han[g], Jong-Seok Moon[g], Jae Man Lee[h], Eun-Gyoung Hong[i], In-Kyu Lee[j], Seong Who Kim[k], Joong Yeol Park[a,b], Sean M. Hartig[e], Un Jung Kang[l], David D. Moore[m], Eun Hee Koh[a,b], and Ki-up Lee[a,b]

[a]Biomedical Research Center, Asan Institute for Life Sciences, Asan Medical Center, University of Ulsan College of Medicine, Seoul, Korea; [b]Department of Internal Medicine, Asan Medical Center, University of Ulsan College of Medicine, Seoul, Korea; [c]Institute for Innovative Cancer Research, Asan Medical Center, University of Ulsan College of Medicine, Seoul, Korea; [d]Convergence Medicine Research Center, Asan Medical Center, University of Ulsan College of Medicine, Seoul, Korea; [e]Molecular and Cellular Biology and Medicine, Division of Diabetes, Endocrinology, and Metabolism, Baylor College of Medicine, Houston, Texas, USA; [f]Laboratory Animal Resource Center, Korea Research Institute of Bioscience and Biotechnology, Daejeon, Korea; [g]Soonchunhyang Institute of Med-bio Science (SIMS), Soonchunhyang University, Korea; [h]Department of Biochemistry and Cell Biology, School of Medicine, Kyungpook National University, Daegu, Korea; [i]Division of Endocrinology and Metabolism, Department of Internal Medicine, Hallym University Dongtan Sacred Heart Hospital, Hallym University College of Medicine, Hwaseong, Korea; [j]Department of Internal Medicine and Biochemistry, Kyungpook National University School of Medicine, Daegu, Korea; [k]Department of Biochemistry and Molecular Biology, University of Ulsan College of Medicine, Seoul, Korea; [l]Department of Neurology, Neuroscience and Physiology, Marlene and Paolo Fresco Institute for Parkinson's and Movement Disorders, NYU Langone Health, New York, USA; [m]Department of Molecular and Cellular Biology, Baylor College of Medicine, Houston, Texas, USA

ABSTRACT

Although macroautophagy/autophagy deficiency causes degenerative diseases, the deletion of essential autophagy genes in adipocytes paradoxically reduces body weight. Brown adipose tissue (BAT) plays an important role in body weight regulation and metabolic control. However, the key cellular mechanisms that maintain BAT function remain poorly understood. in this study, we showed that global or brown adipocyte-specific deletion of *pink1*, a Parkinson disease-related gene involved in selective mitochondrial autophagy (mitophagy), induced BAT dysfunction, and obesity-prone type in mice. Defective mitochondrial function is among the upstream signals that activate the NLRP3 inflammasome. NLRP3 was induced in brown adipocyte precursors (BAPs) from *pink1* knockout (KO) mice. Unexpectedly, NLRP3 induction did not induce canonical inflammasome activity. Instead, NLRP3 induction led to the differentiation of *pink1* KO BAPs into white-like adipocytes by increasing the expression of white adipocyte-specific genes and repressing the expression of brown adipocyte-specific genes. *nlrp3* deletion in *pink1* knockout mice reversed BAT dysfunction. Conversely, adipose tissue-specific *atg7* KO mice showed significantly lower expression of *Nlrp3* in their BAT. Overall, our data suggest that the role of mitophagy is different from general autophagy in regulating adipose tissue and whole-body energy metabolism. Our results uncovered a new mitochondria-NLRP3 pathway that induces BAT dysfunction. The ability of the *nlrp3* knockouts to rescue BAT dysfunction suggests the transcriptional function of NLRP3 as an unexpected, but a quite specific therapeutic target for obesity-related metabolic diseases.

Abbreviations: ACTB: actin, beta; BAPs: brown adipocyte precursors; BAT: brown adipose tissue; BMDMs: bone marrow-derived macrophages; CASP1: caspase 1; CEBPA: CCAAT/enhancer binding protein (C/EBP), alpha; ChIP: chromatin immunoprecipitation; EE: energy expenditure; HFD: high-fat diet; IL1B: interleukin 1 beta; ITT: insulin tolerance test; KO: knockout; LPS: lipopolysaccharide; NLRP3: NLR family, pyrin domain containing 3; PINK1: PTEN induced putative kinase 1; PRKN: parkin RBR E3 ubiquitin protein ligase; RD: regular diet; ROS: reactive oxygen species; RT: room temperature; UCP1: uncoupling protein 1 (mitochondrial, proton carrier); WT: wild-type.

ARTICLE HISTORY
Received 24 September 2019
Revised 24 March 2020
Accepted 3 April 2020

KEYWORDS
Brown adipocyte; inflammasome; pink1; transcriptional activation; white adipocyte

Introduction

Metabolically active brown adipose tissue (BAT) is present in humans [1], and plays an important role in body weight regulation and metabolic control [2,3]. In particular, anatomically defined neck fat isolated from adult human volunteers shares many similarities with classical BAT in rodents [4]. Brown adipocytes are distinct from white adipocytes in that their abundant mitochondria are enriched with UCP1 (uncoupling protein 1), which generates heat from the dissipation of the mitochondrial proton gradient [2]. In addition to brown adipocytes constitutively expressing high levels of UCP1, UCP1-expressing beige adipocytes with thermogenic capacity also develop in white adipose tissue in response to various stimuli [5]. The origin and the transcriptional

CONTACT Eun Hee Koh ehk@amc.seoul.kr Department of Internal Medicine, Asan Medical Center, University of Ulsan College of Medicine, Seoul, Korea; Ki-up Lee kulee@amc.seoul.kr

*These authors contributed equally to this work.

© 2020 The Author(s). Published by Informa UK Limited, trading as Taylor & Francis Group.
This is an Open Access article distributed under the terms of the Creative Commons Attribution-NonCommercial-NoDerivatives License (http://creativecommons.org/licenses/by-nc-nd/4.0/), which permits non-commercial re-use, distribution, and reproduction in any medium, provided the original work is properly cited, and is not altered, transformed, or built upon in any way.

regulation of brown and beige adipocyte development are well characterized [2,5,6]. However, the key cellular mechanisms that maintain BAT mass and function remain poorly understood.

As an important cellular pathway that is activated when nutrients are limited, macroautophagy/autophagy could be expected to counteract the primary energy storage function of white adipocytes. However, targeted deletion of the essential autophagy gene *Atg7* in adipose tissue has been shown to paradoxically result in a lean phenotype in mice [7,8]. A recent study also found that adipocyte-specific *atg5* or *atg12* KO mice are resistant to diet-induced obesity [9]. In that study, autophagy was found to eliminate mitochondria in beige adipocytes during exposure to ADRB3 (adrenergic receptor, beta 3) stimuli or withdrawal from cold exposure.

Deficient mitochondrial quality control results in inflammation and the death of cell populations [10]. Selective autophagy of mitochondria, known as mitophagy, is an important mitochondrial quality control mechanism that eliminates damaged mitochondria [11,12]. Mitophagy selectively removes mitochondria, whereas general autophagy also degrades a range of cytosolic proteins and many types of organelles other than the mitochondria [11,12]. A central mediator of mitophagy is PINK1 (PTEN induced putative kinase 1), a serine-threonine kinase associated with a recessive form of familial Parkinson disease. In the best-characterized pathway to initiate mitophagy, PINK1 activates the E3 ubiquitin ligase PRKN/Parkin to mark depolarized mitochondria for degradation. Interestingly, *PINK1* expression is increased in the muscle and adipose tissues of obese individuals or type 2 diabetes patients [13].

NLRP3 (NLR family, pyrin domain containing 3) inflammasome is an intracellular multiprotein complex that links sensing of microbial products and intracellular danger signals to the proteolytic activation of proinflammatory cytokines [14,15]. Chronic inflammation has been linked to many immune and metabolic diseases, including arthritis, atherosclerosis, diabetes, and aging, and important roles have been described for the NLRP3 inflammasome in all of these pathologies [14–17].

Autophagy/mitophagy blockade activates NLRP3 inflammasomes in macrophages [18,19], and we also found that NLRP3 expression was increased in BAPs from *pink1* knockout mice. Surprisingly, this induction was not associated with the expected activation of the inflammasome function. Rather, previous studies have suggested a quite different function of NLRP3 as a transcriptional regulator [20]. To assess the role of NLRP3 as a mediator of the deleterious effects of loss of PINK1, we generated double *pink1* and *nlrp3* knockouts. The striking reversal of BAT dysfunction in these double knockouts reveals a new mitochondria-NLRP3 pathway that can induce BAT dysregulation.

Results

Pink1 *KO mice manifest BAT dysfunction*

We initially investigated the function of PINK1 in controlling energy balance through monitoring weight gain among *pink1* KO and wild-type (WT) male mice. Eight-week-old male mice were fed a regular diet (RD) or a high-fat diet (HFD) for 8 weeks. The body weight and fat mass of RD-fed mice were not significantly different between the two groups, but we observed a marked increase in weight gain driven by fat mass in HFD-fed *pink1* KO mice (Figure 1A and S1). Interestingly, HFD-fed *pink1* KO mice consumed significantly less food than HFD-fed WT mice (Figure 1B), suggesting that the decrease in energy expenditure (EE) led to the increased weight gain in *pink1* KO mice. RD-fed *pink1* KO mice also consumed significantly less food than RD-fed WT mice (Figure 1B), which may be due to reduced energy demand in response to a decrease in EE. Accordingly, the rates of oxygen consumption (VO_2), CO_2 production (VCO_2), and EE in *pink1* KO mice were significantly lower than those of WT controls (Figure 1C-E, S2A, and S2B). In contrast, locomotor activity was not significantly different between *pink1* KO and WT mice (Figure 1F and S2C), consistent with the findings that dopaminergic neurodegeneration is not found in *pink1* KO mice at 3 to 4 months of age [21]. Interestingly, both RD-fed and HFD-fed *pink1* KO mice showed insulin resistance, even though the body weight was not significantly higher in RD-fed *pink1* KO mice. (Figure 2).

Given the considerable influence of BAT on overall energy balance [2], we investigated morphological differences in tissue architecture between *pink1* KO and WT controls. BAT from control mice showed prototypically small and multilocular lipid droplets at 8 and 16 weeks of age (Figure 3A and B). *pink1* KO mice exhibited a "whitening" of BAT (i.e., the transformation of brown fat cells to cells having large and unilocular lipid droplets). HFD feeding in *pink1* KO mice further increased BAT whitening [22] (Figure 3A and B). Electron microscopy examination showed ballooning of the mitochondrial matrix and disorganized cristae in *pink1* KO brown adipocytes (Figure 3C and D).

The UCP1 in BAT dissociates respiration from ATP formation and generates heat to regulate whole-body EE [23]. In *pink1* KO mice, UCP1 expression in BAT was significantly lower than in WT mice (Figure 3E and S3). To examine the effect of PINK1 deletion on thermogenesis, we monitored the body temperatures of the mice after cold exposure. Body temperatures of *pink1* KO mice were not significantly different from those of WT mice at room temperature (RT). However, after cold exposure at 4°C for 6 h, *pink1* KO mice had significantly lower body temperatures than WT mice (Figure 3F). Mitochondrial biogenesis and mitophagy represent two opposing but coordinated processes that regulate mitochondrial content, structure, and function [24]. The expression of *Ppargc1a* (peroxisome proliferative activated receptor, gamma, coactivator 1 alpha), the master regulator of mitochondrial biogenesis [24], was significantly lower in the BAT of *pink1* KO mice, and this was associated with lower expressions of brown adipocyte-specific markers (Figure 3G).

To establish how PINK1 ablation impacts beige fat thermogenesis, we injected WT and *pink1* KO mice with the ADRB3 agonist (CL-316243). The inguinal adipose tissue of WT and *pink1* KO mice showed similarly increased expression of UCP1, suggesting that the changes in *pink1* KO mice are limited to classical brown adipocytes (Figure 4).

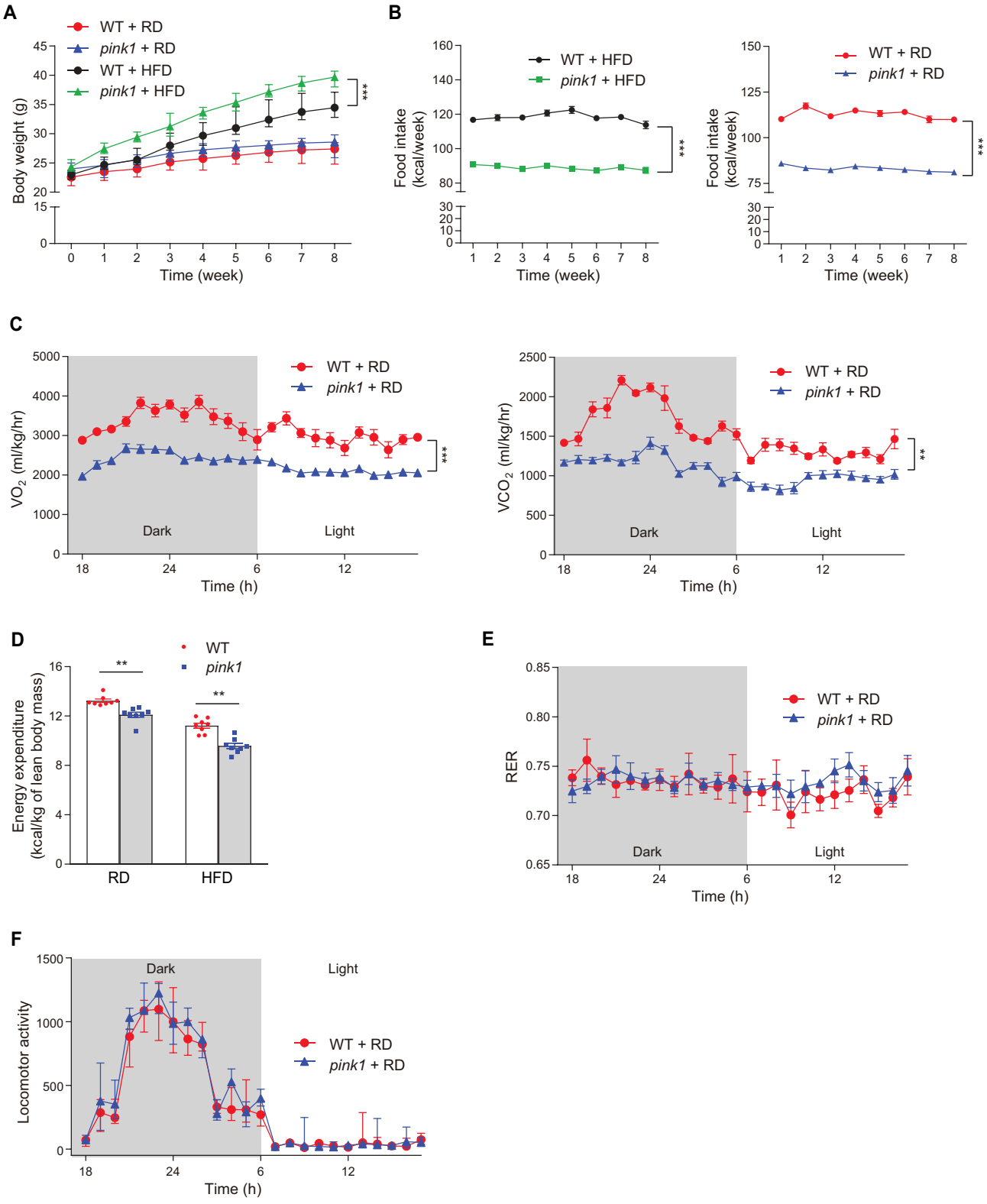

Figure 1. Decreased energy expenditure in *pink1* KO mice. (A) Body weight of *pink1* KO (*pink1*) mice and WT littermates fed RD or HFD ($n = 13$). (B) Average daily food intake per mouse ($n = 13$). (C-F) Decreased EE in *pink1* KO mice. (C) O_2 consumption and CO_2 production ($n = 8$). (D) EE was calculated as (3.815 + 1.232 × RER) × VO_2/lean mass ($n = 8$). (E) RER and (F) locomotor activity ($n = 8$). Data are presented as mean ± SEM. Student's two-tailed unpaired *t*-test (D) or one-way repeated-measures ANOVA (A-C, E and F); $^{**}p < 0.01$, $^{***}p < 0.001$.

Pink1 *KO BAPs differentiate into white-like adipocytes*

We then examined the mechanism of BAT dysfunction in *pink1* KO mice using brown adipocyte precursors (BAPs) isolated from the stromal vascular fraction of the interscapular BAT [25]. Tissue-specific precursor/stem cells are required for the maintenance of physiological and regenerative responses [26], and deterioration in their function underlies aging-related BAT dysfunction [27]. We

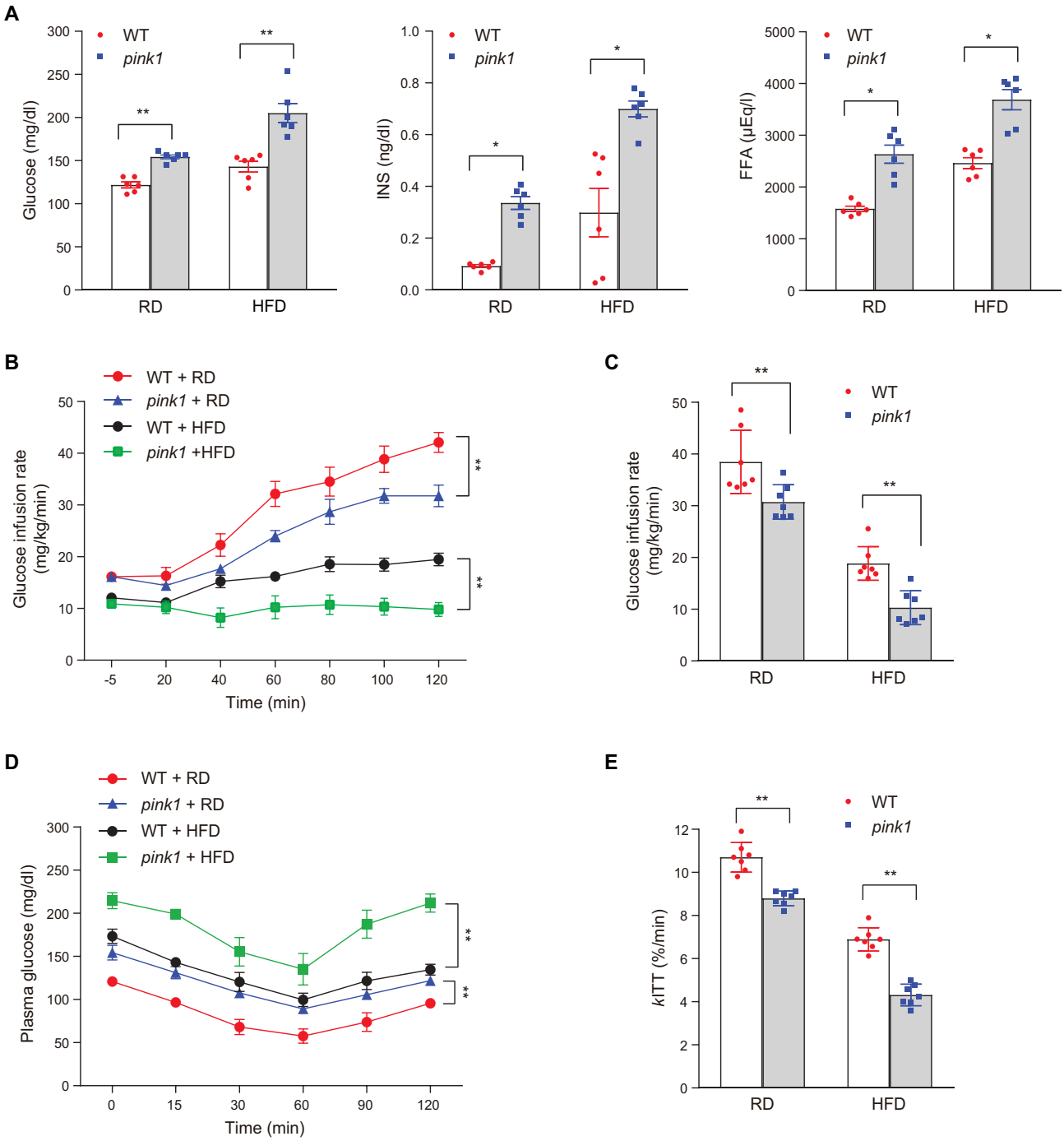

Figure 2. Insulin resistance in *pink1* KO mice. (A) Fasting plasma glucose, INS, and free fatty acid (FFA) levels in *pink1* KO mice ($n = 6$). (B) Glucose infusion rate (GIR) in the euglycemic hyperinsulinemic clamp studies ($n = 7$). (C) Mean GIR values from 80 to 120 min ($n = 7$). (D) ITT ($n = 7$). (E) Glucose disappearance rate for ITT (*k*ITT; %/min) ($n = 7$). Data are presented as mean ± SEM. Student's two-tailed unpaired *t*-test (A, C and E) or one-way repeated-measures ANOVA (B, D); $^{*}p < 0.05$, $^{**}p < 0.01$.

noted that differentiation of BAPs derived from *pink1* KO mice was defective, as grossly reflected by larger lipid droplets (Figure 5A-C) and significantly decreased levels of *Ucp1* and brown adipocyte-specific marker genes (Figure 5D). On the other hand, the expression levels of white adipocyte-specific genes were significantly increased in *pink1* KO BAPs (Figure 5E).

Mitophagy can be estimated by several methods, such as the recruitment of PRKN (parkin RBR E3 ubiquitin protein ligase) to chemically depolarized mitochondria, or using MitoTimer, a fluorescent probe that investigates mitochondrial turnover on the subcellular level [28]. Recently, a pH-sensitive, dual-excitation, ratiometric, mitochondrial-targeted, fluorescent protein – mt-Keima – was described that also exhibits resistance to lysosomal proteases [29]. At the physiological pH of the mitochondria (pH 8.0), shorter-wavelength excitation predominates. Within the acidic lysosome (pH 4.5) after mitophagy, mt-Keima undergoes a gradual shift to

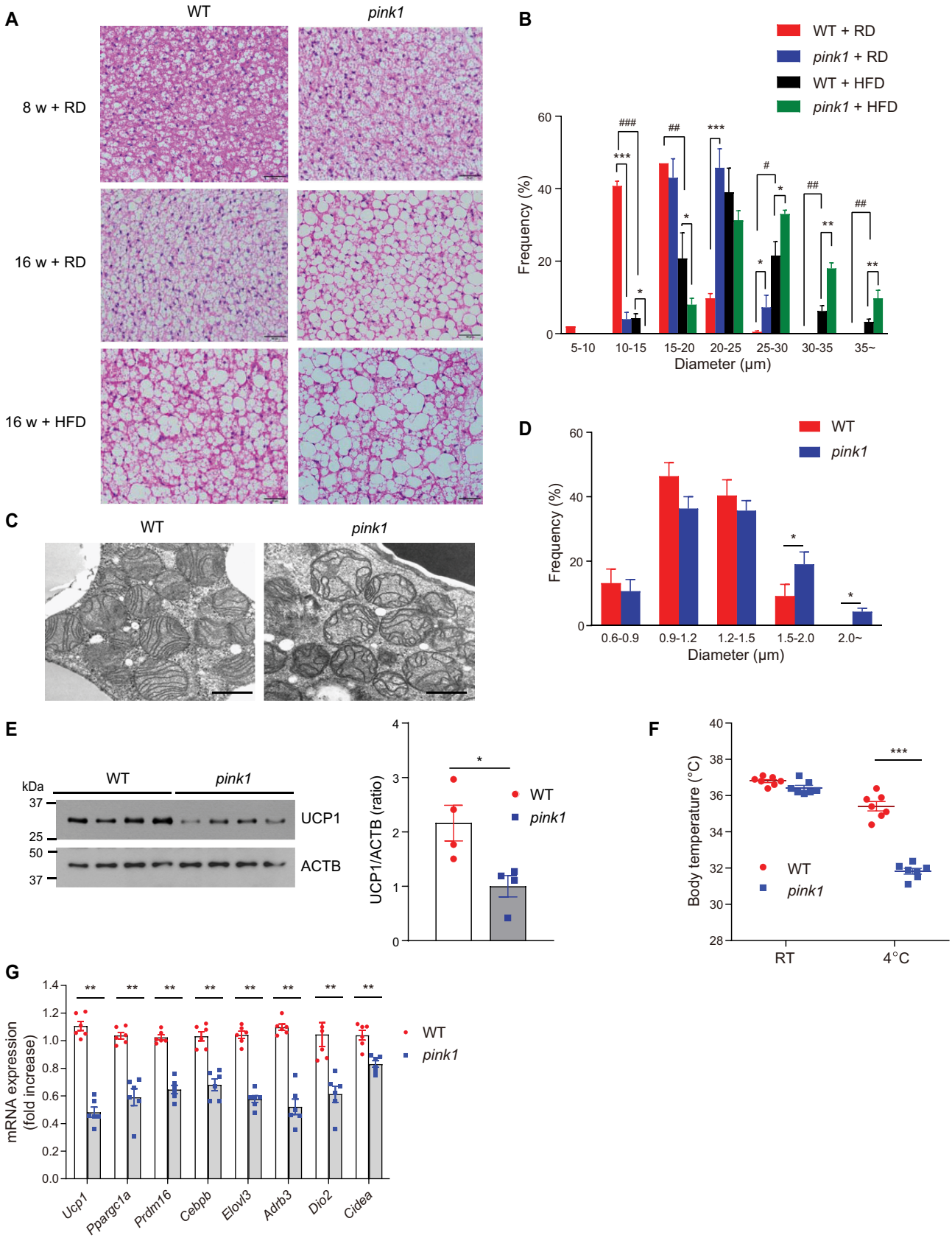

Figure 3. Brown fat dysfunction in *pink1* KO mice. (A and B) H&E stained BAT sections. Scale bar: 50 μm (A). Average sizes of adipocytes in H&E sections of 16-weeks-old mice measured by ImageJ (B). For each mouse, 10 fields of H&E sections were randomly selected for analysis ($n = 4$). (C and D) Transmission electron micrographs of BAT revealing the ballooning of the mitochondrial matrix and disorganized mitochondrial cristae in *pink1* KO mice ($n = 4$). Scale bar: 1 μm. (D) Morphometric analysis of TEM images performed with ImageJ on a sample of 10 randomly selected images from 4 mice. (E) Representative western blots of UCP1 protein in BAT from 3 independent experiments are shown (left panel). Equal amounts of protein (30 μg) were loaded in each lane, and the exposure times for detecting UCP1 and ACTB were both 30 s. See **Fig. S3** for details. The intensities of UCP1 were quantified using the ImageJ software and compared with that of ACTB (right panel). (F) Core temperature in mice at RT and after exposure to 4°C for 6 h ($n = 7$). (G) mRNA expression of brown adipocyte-specific genes ($n = 6$). Data are presented as mean ± SEM. One-way ANOVA with Bonferroni correction for post hoc analysis (B) or Student's two-tailed unpaired *t*-test (D-G). $^{*}p < 0.05$, $^{**}p < 0.01$, $^{***}p < 0.001$ vs WT; $^{\#}p < 0.05$, $^{\#\#}p < 0.01$, $^{\#\#\#}p < 0.001$ vs RD.

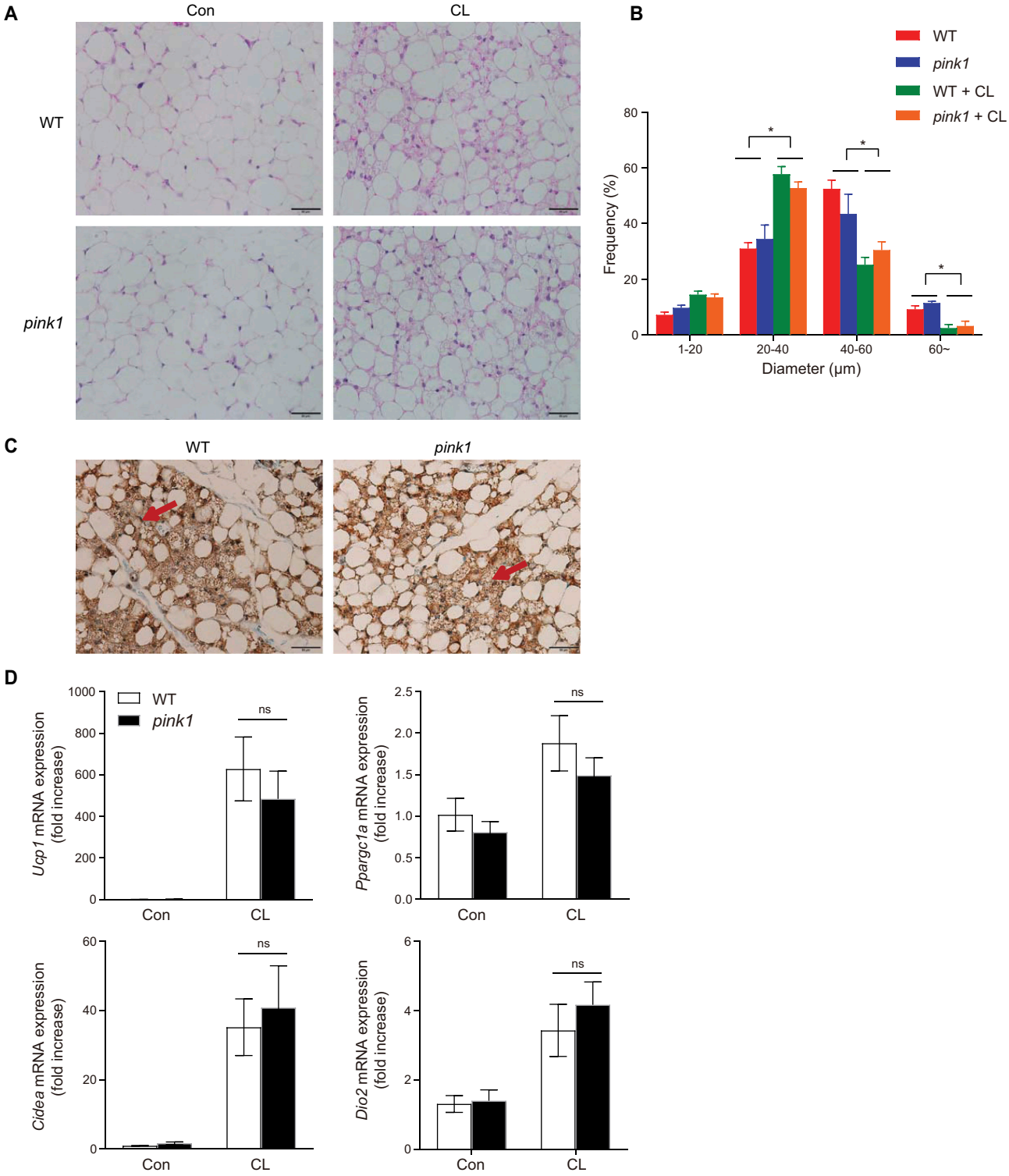

Figure 4. Effects of the ADRB3 agonist on thermogenic gene induction in inguinal WAT (iWAT). Eight-weeks-old male WT and *pink1* KO mice received daily intraperitoneal injections of CL-316,243 (CL) for 3 d. (A) H&E staining of iWAT. Scale bar: 50 μm ($n = 4$). Average sizes of adipocytes in H&E sections of 16-weeks-old mice measured by ImageJ (B). For each mouse, 10 fields of H&E sections were randomly selected for analysis. (C) Immunohistochemical staining of UCP1-positive adipocytes. Arrows indicate UCP1 staining in the iWAT. Scale bar: 50 μm ($n = 4$). (D) *Ucp1* and thermogenic gene expression ($n = 6$). Data are presented as mean ± SEM. One-way ANOVA with Bonferroni correction for post hoc analysis (B) or Student's two-tailed unpaired *t*-test (D). *$p < 0.05$ versus CL-untreated mice, ns; not significant.

longer-wavelength excitation [29]. As expected, *pink1* KO BAPs showed defective mitophagy (Figure 5F and S4), and this was associated with increased mitochondrial ROS generation (Figure 5G).

Increased NLRP3 expression in pink1 *KO BAPs is not associated with inflammasome activation*

Inflammasomes are multiprotein complexes that activate CASP1 (caspase 1), which induces the maturation of the

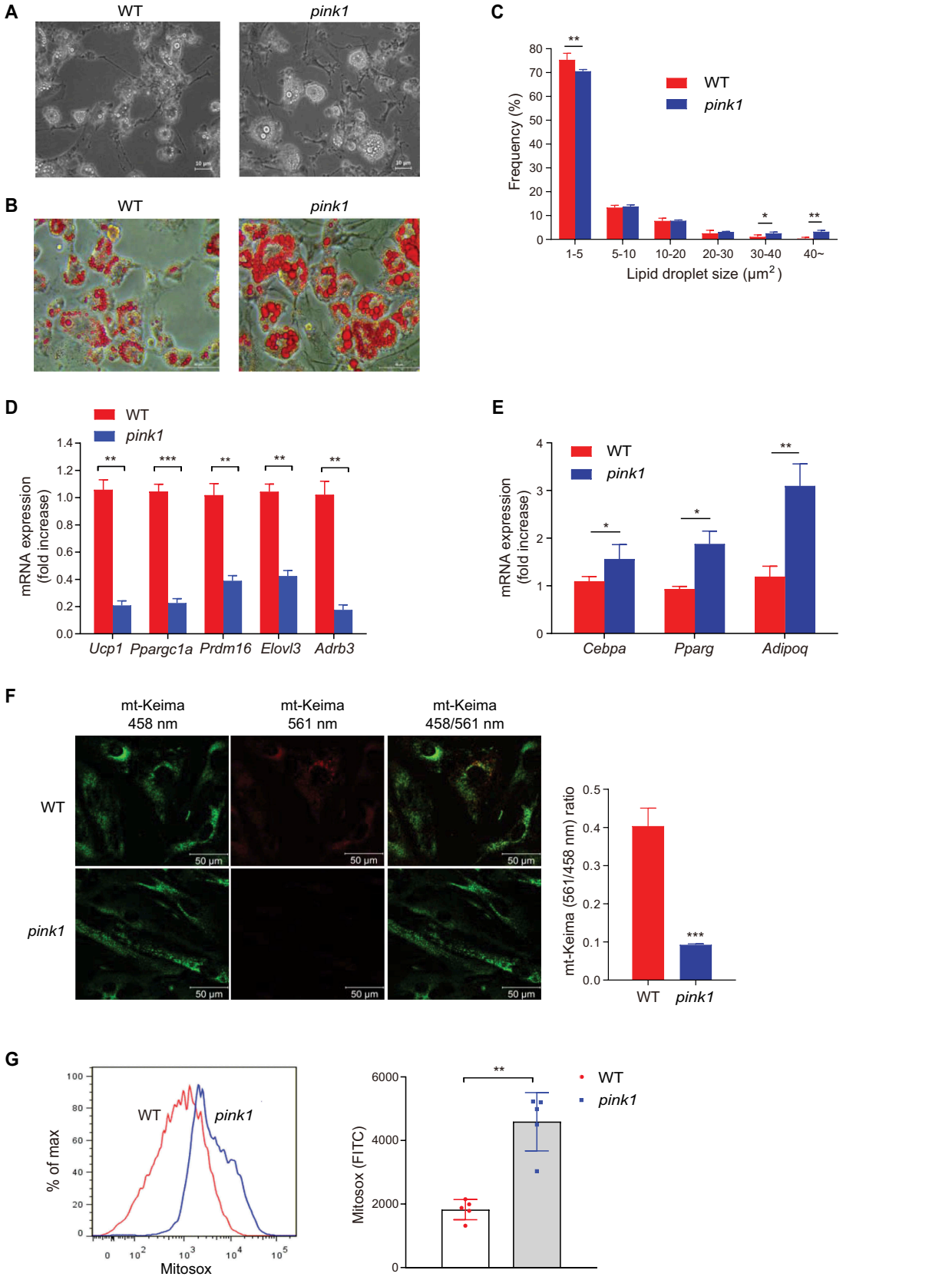

Figure 5. BAPs of *pink1* KO fail to differentiate into brown adipocytes. (A-C) BAPs obtained from the stromal vascular fraction of interscapular BAT of WT and *pink1* KO mice were differentiated into brown adipocytes. After 7 d of differentiation, adipocytes were fixed, and the lipid droplets were stained with Oil Red O solution. (A) Phase-contrast fields. Scale bar: 50 μm ($n = 4$). (B and C) Oil-red O micrographs of differentiated brown adipocytes. Lipid droplet area was measured with ImageJ. For analysis, 10–12 fields in each slide were randomly selected. Scale bar: 10 μm ($n = 4$). (D and E) mRNA expression levels of brown adipocyte-specific genes (D) and white adipocyte-specific genes (E) in differentiated brown adipocytes ($n = 6$). (F) Estimation of mitophagy by mt-Keima method in WT and *pink1* KO BAPs. The ratio of fluorescence intensity in mt-Keima staining (458 nm) and mitochondria fused with the lysosome (561 nm) was measured using ImageJ ($n = 9$). (G) Measurements of mitochondrial ROS by flow cytometry using mitochondrial superoxide probe MitoSox Red. Quantitative analysis of MitoSox Red fluorescence intensity ($n = 5$). Data are presented as mean ± SEM. Student's two-tailed unpaired *t*-test (C-G). *$p < 0.05$, **$p < 0.01$, ***$p < 0.001$.

proinflammatory cytokines, IL1B (interleukin 1 beta) and IL18 (interleukin 18). Autophagy/mitophagy blockade activates NLRP3 inflammasomes in macrophages [18,19]. However, NLRP3 protein and inflammasome activity are also present in non-myeloid cells [30–32]. We observed NLRP3 expression was significantly higher in the BAPs of *pink1* KO mice (Figure 6A, 6B, and S5A). Interestingly, however, the increased NLRP3 expression in the BAPs isolated from *pink1* KO mice did not correlate with the canonical measures of inflammasome activity. Thus, CASP1 cleavage or IL1B secretion (Figure 6C, 6D, 6F, S5B, and S5D) was not observed in BAPs incubated with lipopolysaccharide (LPS) and ATP. In contrast, bone marrow-derived macrophages (BMDMs) stimulated with LPS and ATP showed CASP1 cleavage and IL1B secretion into the supernatant, and this was significantly higher in the BMDMs of *pink1* KO mice than of WT mice (Figure 6C, 6E, 6F, S5C, and S5E). These findings indicate that while inflammasome-dependent NLRP3 activation occurs in *pink1* KO BMDMs, this response does not occur in BAPs.

NLRP3 induces white-like adipocytes in pink1 *KO BAPs*

in addition to acting as an intracellular complex for cytokine maturation, NLRP3 can act as a transcription factor [20]. The sequence 5′-nGRRGGnRGAG-3′ (where 'n' is any nucleotide and 'R' is any purine) has been suggested as the consensus motif for NLRP3 binding [20]. The transcription factor CEBPA (CCAAT/enhancer binding protein [C/EBP], alpha) plays an essential role in the differentiation and maintenance of WAT [33-35]. We found that *Cebpa* contains the NLRP3 consensus motif in its promoter regions (Figure 7A), and the chromatin immunoprecipitation (ChIP) assay revealed that NLRP3 binding near the *Cebpa* was higher in both undifferentiated and differentiated BAPs from *pink1* KO mice (Figure 7B). To examine whether NLRP3 can induce white-like adipocytes, we introduced *Nlrp3* into WT BAPs using lentiviral vectors. As expected, NLRP3 induced the expression of *Cebpa*, and *Pparg* (peroxisome proliferator activated receptor gamma) and *Adipoq* (adiponectin, C1Q and collagen domain containing), white adipocyte-specific genes that are regulated by *Cebpa* [36-38]. NLRP3 also repressed the expression of brown adipocyte-specific genes (Figure 7C and D). Conversely, *Pink1* overexpression in *pink1* KO BAPs reversed defective mitophagy (Figure 7E) and decreased the expression of *Nlrp3* (Figure 7F), which was associated with the reversal of the aforementioned changes in white and brown fat-specific markers (Figure 7G and H). Based on these results, we suggest that NLRP3 transcriptionally regulates BAPs in *pink1* KO mice.

BAT changes in pink1 *KO mice are reversed in* pink1 nlrp3 *double-KO mice*

To test whether the induction of NLRP3 is an important mediator of BAT dysfunction in *pink1* KO mice, we generated mice deficient for both *pink1* and *nlrp3*. Changes in VO_2 and VCO_2 in *pink1* KO mice were almost completely reversed in *pink1 nlrp3* double-KO mice (Figure 8A). BAT changes in *pink1* KO mice were also reversed in *pink1 nlrp3* double-KO mice (Figure 8B-D, S6A, and S6B), whereas *pink1 casp1* double-KO mice did not show such reversal (Figure 8E and S6C).

Likewise, BAPs isolated from *pink1 nlrp3* double-KO mice exhibited normal differentiation into mature brown adipocytes (Figure 8F, 8G, and S6D), indicating that NLRP3 hinders BAT development in *pink1* KO mice.

Pink1 *deficiency in brown adipocytes induces brown fat dysfunction but not insulin resistance*

To test whether defective mitophagy in brown adipocytes *per se* or that in macrophages is responsible for BAT dysfunction, we produced brown adipocyte-specific (*pink1* $^{f/f}$*-Ucp1*-Cre) and myeloid-specific *pink1* KO mice (*pink1* $^{f/f}$*-Lyz2*-Cre). Brown adipocyte-specific *pink1* KO mice (but not myeloid cell-specific *pink1* KO mice) showed VO_2, VCO_2, EE, morphologic features, and gene expression profiles of BAT similar to those of *pink1* global KO mice (Figure 9A-D). Brown adipocyte-specific *pink1* KO mice also had significantly lower body temperatures than did WT mice after cold exposure at 4°C for 6 h (Figure 9E).

We then performed an insulin tolerance test (ITT) in brown adipocyte-specific *pink1* KO mice to test whether brown adipocyte mitophagy contributes to insulin sensitivity. We found that brown adipocyte-specific *pink1* KO mice did not show alterations in INS (insulin) sensitivity (Figure 9F and G), indicating that brown adipocyte mitophagy contributes to the maintenance of energy expenditure but not of INS sensitivity.

Discussion

When dysfunctional mitochondria are not cleared adequately by mitophagy/autophagy, this leads to aging-associated diseases, including obesity [10]. PINK1 was originally linked to Parkinson disease, but no substantial Parkinson disease-relevant phenotypes are observed in *pink1* KO mice [21]. However, a recent study found that vigorous exercise and mitochondrial DNA mutations lead to inflammation through the CGAS (cyclic GMP-AMP synthase)-STING1 (stimulator of interferon response cGAMP interactor 1) pathway in these mice [39]. Our study newly shows that PINK1-mediated mitophagy is essential for maintaining the function of BAT, in which mitochondria are abundant.

The effects of mitophagy that we observed corroborate the recent results that showed cold-induced induction of mitophagy in BAT [40]. Our study is also consistent with recent research demonstrating defective mitophagy, BAT dysfunction, and insulin resistance in mice with adipocyte-specific deletion of AMP-activated protein kinase [41]. However, in adipocytes, the ablation of mitophagy (*Pink1*) yielded contrasting effects to the ablation of autophagy (*Atg7*) on diet-induced obesity; the latter results in the lean phenotype after HFD feeding [7,8]. To explain the lean phenotype of adipose-*atg7* KO mice, it was proposed that *Atg7* plays important roles in normal adipogenesis and that inhibition of autophagy affects white adipocyte differentiation, thereby leading to the lean phenotype [7,8]. In addition, *atg7* KO mice showed increased BAT mass [8]. Such seemingly discrepant results may be explained by the fact that adipocyte-specific *atg7* KO mice showed

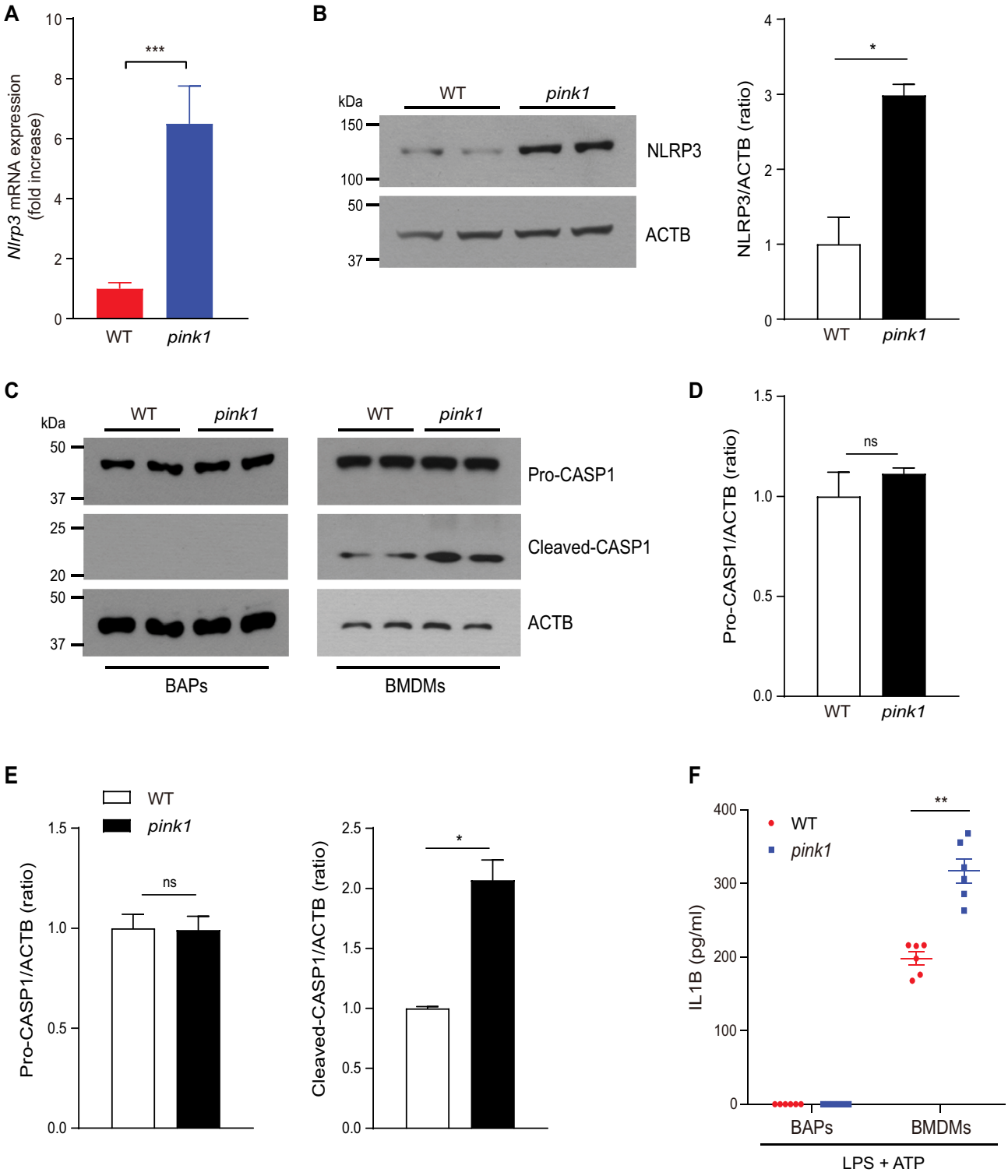

Figure 6. Increased NLRP3 expression in *pink1* KO BAPs is not associated with inflammasome activation. (A) mRNA expression ($n = 6$) and (B) representative western blots of NLRP3 in the BAPs of WT and *pink1* KO mice from 3 independent experiments are shown. Equal amounts of protein (10 μg) were loaded in each lane, and the exposure times for detecting NLRP3 and ACTB were both 2 min. See **Fig. S5A** for details. The level of NLRP3 was quantified using the ImageJ software and compared with that of ACTB. (C) Immunoblot of cleaved-CASP1. LPS-primed (100 ng/ml for 4 h) BAPs and BMDMs from WT or *pink1* KO mice were stimulated with ATP (5 mM for 30 min). Representative blots from 3 replicated independent experiments are shown. (D) Equal amounts of protein (10 μg) were loaded in each lane, and the exposure times for detecting CASP1 and ACTB in BAPs were 5 min and 2 min, respectively. See **Fig. S5B and S5D** for details. (E) The exposure times for detecting pro-CASP1, cleaved-CASP1, and ACTB in BMDMs were 30 s, 30 min, and 30 s, respectively. See **Fig. S5 C and S5E** for details. (F) ELISA measurement of IL1B levels of supernatants after LPS and ATP treatment ($n = 6$). Data are presented as mean ± SEM. Student's two-tailed unpaired *t*-test; $^{*}p < 0.05$, $^{**}p < 0.01$, $^{***}p < 0.001$, ns; not significant.

significantly lower expression of *Nlrp3* in their BATs compared with those of control mice (Figure S7). The cause of this decrease in *Nlrp3* is unclear.

A recent study found that autophagy eliminates mitochondria in beige adipocytes during withdrawal from cold exposure or ADRB3 stimuli [9]. By using adipocyte-

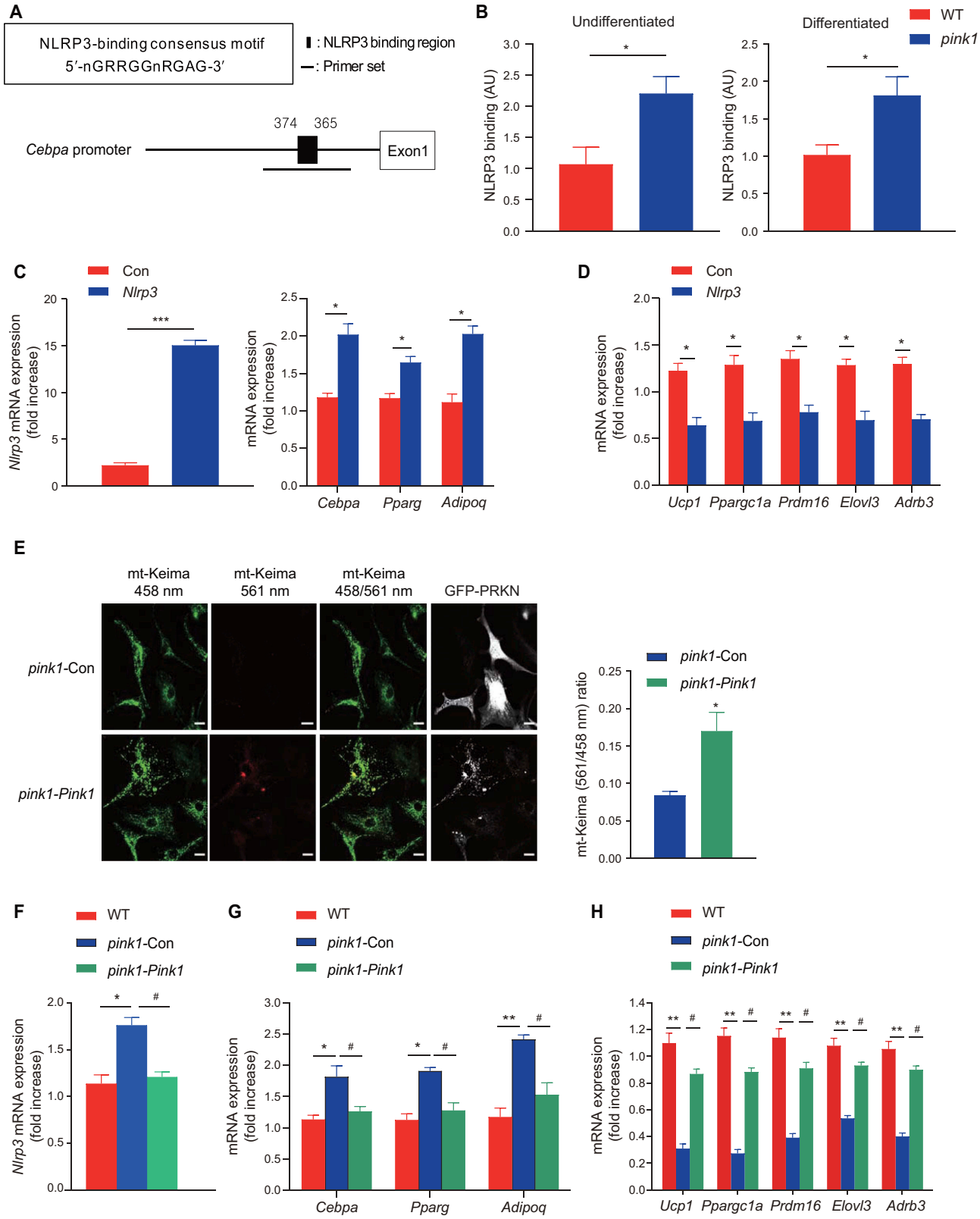

Figure 7. Increased *Nlrp3* in BAPs from *pink1* KO mice transcriptionally activates white adipocyte-like differentiation. (A and B) Binding of NLRP3 to the promoter regions of *Cebpa*. ChIP assay was performed to assess the NLRP3 binding sites in the nt −374 to −365 region of the *Cebpa* promoter. Four independent experiments were performed. Undifferentiated BAPs or 5 d post-differentiation BAPs were used in the ChIP assay. (C and D) Effect of overexpression of *Nlrp3* in WT BAPs on the expression of *Nlrp3*, white adipocyte- (C), and brown adipocyte-specific markers (D). BAPs were transfected with a lentivirus carrying *Nlrp3* or control vector (Con) and harvested 7 d after differentiation ($n = 6$). (E-H) Rescue of mitophagy by overexpression of *Pink1* in *pink1* KO BAPs. *pink1* KO BAPs were transfected with lentiviruses for *pink1* (*pink1-Pink1*) or control vector (*pink1*-Con). (E) Estimation of mitophagy by mt-Keima method. The ratio of fluorescence intensity in mt-Keima staining (458 nm) and mitochondria fused with the lysosome (561 nm) was measured using ImageJ ($n = 4$). (F-H) mRNA expressions of *Nlrp3* (F), white adipocyte markers (G) and brown adipocyte (H) ($n = 6$). Data are presented as mean ± SEM. Student's two-tailed unpaired *t*-test (B-E); $^{*}p < 0.05$, $^{***}p < 0.001$. One-way ANOVA with Bonferroni correction for post hoc analysis (F-H); $^{*}p < 0.05$, $^{**}p < 0.01$ vs WT BAPs; $^{\#}p < 0.05$ vs *pink1* KO BAPs.

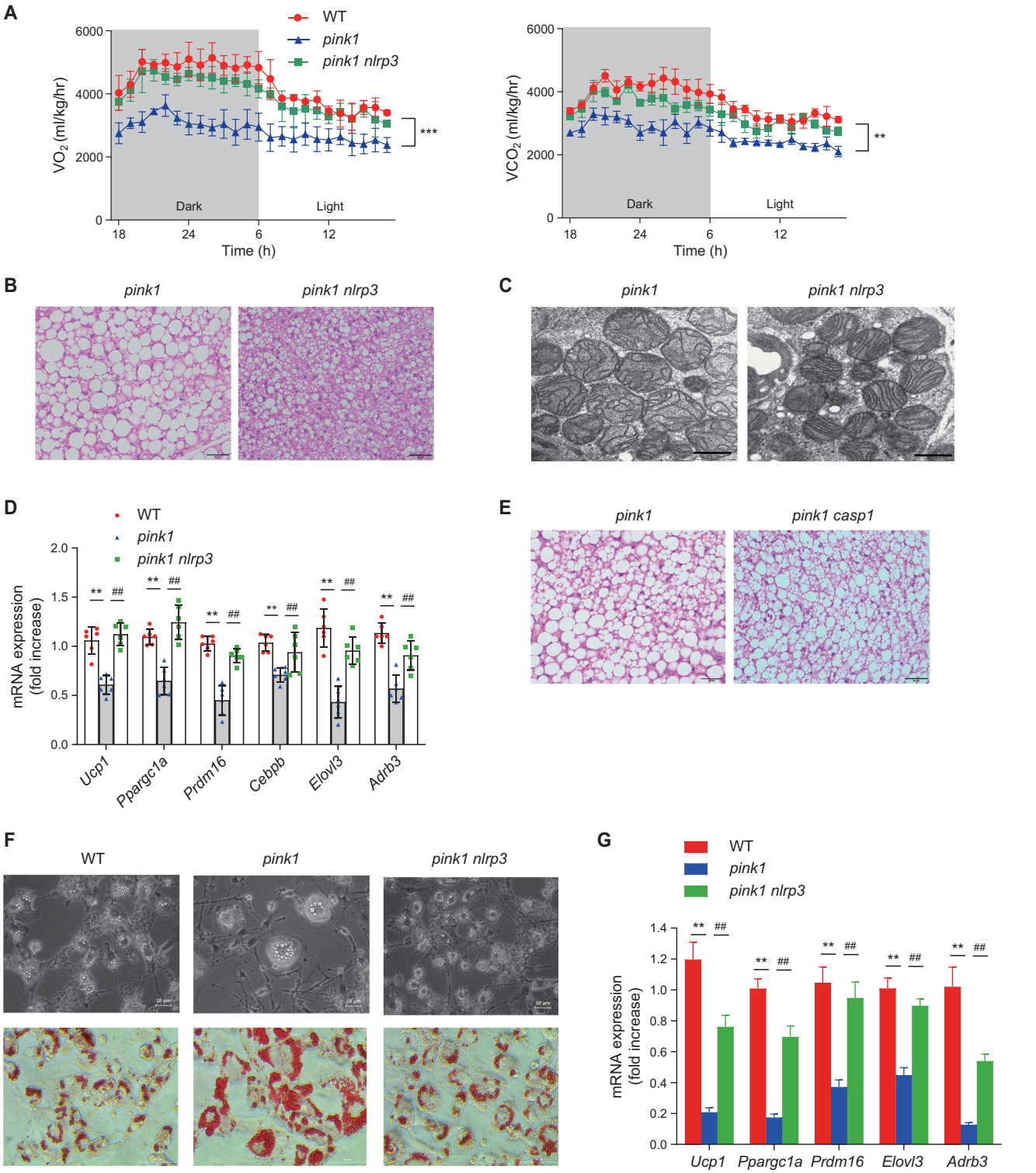

Figure 8. BAT changes in *pink1* KO mice are reversed in the *pink/nlrp3* double-KO mice. (A-D) Eight-week-old male mice in each group were fed RD for 8 weeks. Gas exchange (A), H&E staining of BAT in *pink1 nlrp3* double-KO mice (*pink1 nlrp3*) ($n = 4$). Scale bar: 50 μm (B), and representative transmission electron micrograph of BAT from *pink1* KO and *pink1 nlrp3* double-KO mice ($n = 4$). Bar: 1 μm (C). mRNA expression of BAT-specific genes in the BAT ($n = 6$) (D). (E) H&E staining of BAT in *pink1 casp1* double-KO (*pink1 casp1*) mice ($n = 4$). Scale bar: 50 μm. Data are presented as mean ± SEM. One-way repeated-measures ANOVA with Bonferroni correction for post hoc analysis (A) or one-way ANOVA with Bonferroni correction for post hoc analysis (D); $^{**}p < 0.01$, $^{***}p < 0.001$ vs. WT; $^{\#\#}p < 0.01$ vs. *pink1* KO mice. (F and G) Reversal of defective differentiation to mature brown adipocytes in *pink1 nlrp3* KO BAPs. (F) Phase-contrast microscopy (top) and Oil-Red O (down) images were showing the reversal of morphologic changes in differentiated brown adipocytes obtained from *pink1 nlrp3* double-KO mice ($n = 4$). After 7 d of differentiation, images were obtained. Scale bar: 5 μm (phase-contrast) and 50 μm (Oil-Red O). (G) mRNA expression of BAT markers in the BAPs ($n = 6$). Data are presented as mean ± SEM. One-way ANOVA with Bonferroni correction for post hoc analysis. $^{**}p < 0.01$ vs WT BAPs; $^{\#\#}p < 0.01$ vs *pink1* KO BAPs.

specific *atg5* or *atg12* KO mice, the authors showed that autophagy deficiency leads to the resistance to diet-induced obesity. In another study, the same group showed that PRKN-dependent mitophagy is upstream of autophagy-induced mitochondrial clearance [42]. The cause of this discrepancy is unclear, but the role of mitophagy may be

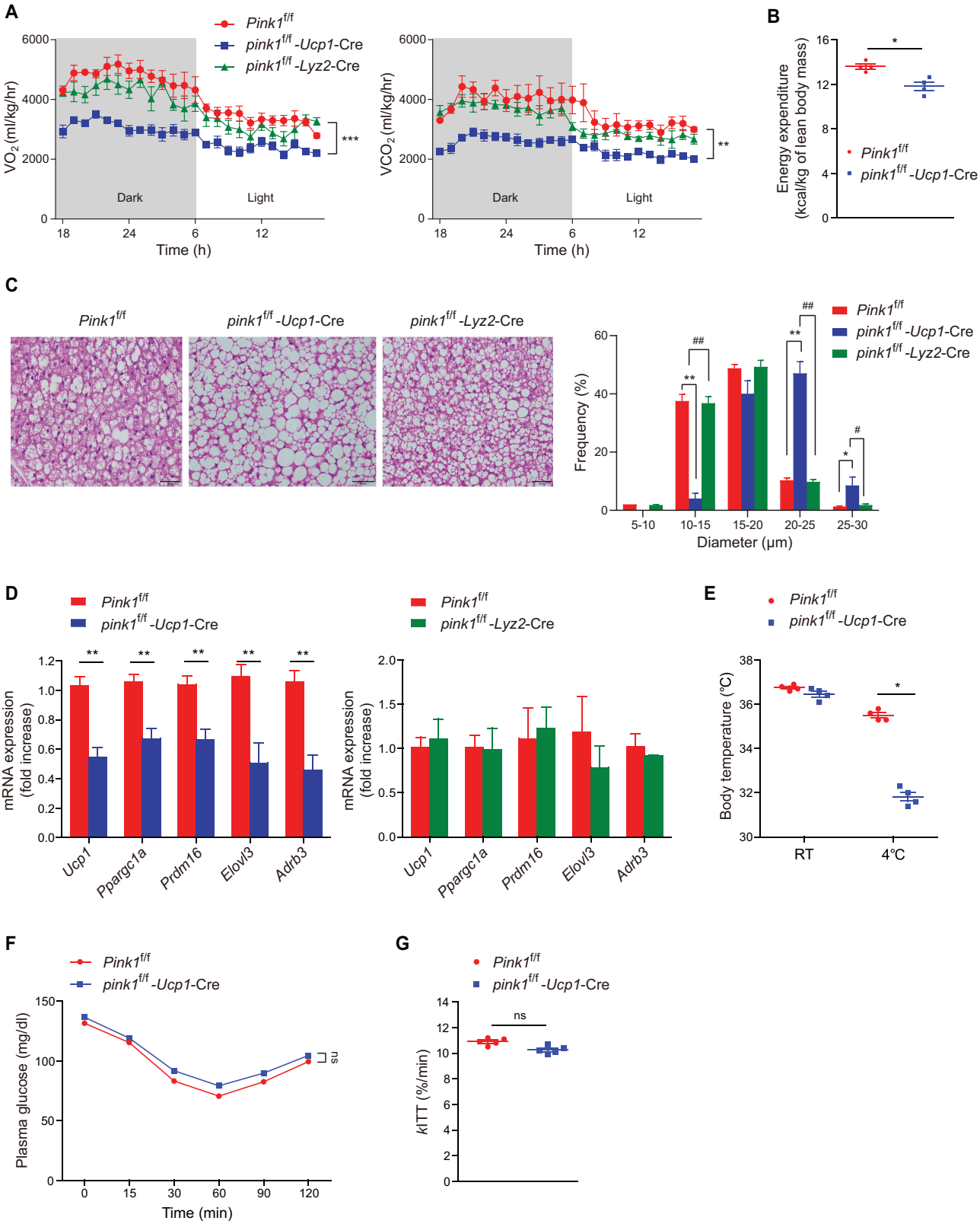

Figure 9. *Pink1* deficiency in brown adipocytes is sufficient to induce brown fat dysfunction. (A) O_2 consumption and CO_2 production in brown fat-specific (*pink1* $^{f/f}$-*Ucp1*-Cre) or myeloid cell-specific (*pink1* $^{f/f}$-*Lyz2*-Cre) *pink1* KO mice ($n = 4$). (B) EE in *pink1* $^{f/f}$-*Ucp1*-Cre *pink1* KO mice and *Pink1* $^{f/f}$ mice ($n = 4$). (C) H&E staining of BAT. Scale bar: 50 μm ($n = 4$). (D) mRNA expression levels of brown fat-specific genes ($n = 4$). (E) Core temperature in *pink1* $^{f/f}$-*Ucp1*-Cre *pink1* KO mice and *Pink1* $^{f/f}$ mice at RT and after exposure to 4°C for 6 h ($n = 4$). (F and G) ITT (F) and glucose disappearance rate for ITT (*k*ITT; %/min) (G) in *pink1* $^{f/f}$-*Ucp1*-Cre *pink1* KO mice ($n = 5$). Data are presented as mean ± SEM. One-way repeated-measures ANOVA (A and F), or One-way ANOVA with Bonferroni correction for post hoc analysis (C) or Student's two-tailed unpaired *t*-test (B, D, E and G); $^{*}p < 0.05$, $^{**}p < 0.01$, $^{***}p < 0.001$ vs *Pink1* $^{f/f}$, $^{\#}p < 0.05$, $^{\#\#}p < 0.01$ vs *pink1* $^{f/f}$-*Ucp1*-Cre; ns, not significant.

different between the lineages of brown and beige adipocytes, considering that the two cell types arise from divergent precursor cells [2,43].

in this study, we show that NLRP3 expression was increased in the BAPs of *pink1* KO mice and that this led to BAT dysfunction. In addition to its role as an intracellular

sensor that detects microbial products and endogenous danger signals to activate NLRP3 inflammasome, NLRP3 can induce the differentiation of white-like adipocytes from BAPs. While targeting of NLRP3 as a therapeutic for multiple diseases is rapidly progressing, current treatment focuses on inhibition of the inflammasome-derived cytokine IL1B [44]. However, it was pointed out that directly targeting NLRP3 by small molecules is specific, cost-effective, and less invasive than the cytokine blockade [44]. In this regard, our study showing the transcriptional function of NLRP3 provides an additional rationale for directly targeting NLRP3 for obesity-related metabolic diseases.

BAT possesses a large capacity for glucose uptake and metabolism, and an ability to regulate insulin sensitivity [45]; however, RD-fed brown adipocyte-specific *pink1* KO mice showed normal results in ITT, whereas RD-fed global *pink1* KO mice showed insulin resistance. This discrepancy suggests that brown adipocyte mitophagy contributes to the maintenance of energy expenditure but not of insulin sensitivity, and that other tissues or organs might contribute to the insulin resistance in global *pink1* KO mice. Further studies are warranted to examine the possible role of mitophagy in other INS target tissues (i.e., skeletal muscle, liver, and white adipose tissue) in the generation of insulin resistance [46].

in summary, our data suggest that the role of mitophagy is different from general autophagy in regulating adipose tissue and whole-body energy metabolism. Our data show that mitophagy plays a crucial role in maintaining the BAT function and energy metabolism of the whole body. *pink1* deficiency increased NLRP3 to induce white-like adipocytes from BAPs, and this led to brown fat dysfunction. Therefore, in addition to its role in Parkinson disease, PINK1 may act as a target for managing metabolic diseases associated with obesity. In particular, the transcriptional function of NLRP3 may be an unexpected, but quite specific therapeutic target for metabolic diseases.

Materials and methods

Mice

All mice were housed in ambient RT (22 ± 1°C) with 12/12 h light-dark cycles and free access to water and food. Eight-week-old male mice in each group were given RD or HFD (Research Diets, Inc, D12492) and were sacrificed after feeding for 8 weeks. All animal experiment protocols were approved by the Institutional Animal Care and Use Committee of the Asan Institute for Life Sciences, Seoul, Korea.

Generation of KO mouse lines

The *pink1* KO mouse line has been described previously [47]. Breeding pairs were obtained from the Mary Lyon Centre at the MRC Harwell Institute, Oxfordshire, UK. *pink1 nlrp3* double-KO mice were generated using the TALEN method, as described elsewhere [48] (**Table S1**). The *pink1 casp1* double-KO mice strain was generated by crossing *pink1* KO and *casp1* KO mice (Jackson Laboratory, 016621). Myeloid cell-specific and brown fat-specific *pink1* KO mice were generated by crossing floxed *pink1* mice (European Mouse Mutant Archive, EM:07320) with *Lyz2* (Jackson Laboratory, 004781) and *Ucp1* Cre mice (Jackson Laboratory, 024670), respectively. First, WT/del (F1) and WT/flox (F1) mice were generated by cross-breeding WT/flox mice and Cre mice. Then, del/del, flox/flox, and WT/WT mice were generated by cross-breeding within the F1 generation.

atg7 flox/flox mice of C57BL/6 background were kindly provided by Dr. Komatsu at Niigata University, Japan. *atg7* flox/flox mice and *Fabp4* Cre mice (Jackson Laboratory, 005069) were crossed to produce adipose-*atg7* KO mice [8].

Indirect calorimetry

VO_2, VCO_2, RER, and locomotor activity were assessed using an eight-chamber Oxymax system (Columbus Instruments). Mice were placed in the chambers at 23°C with free access to food and water and acclimated for more than 50 min before measurement. EE was calculated as (3.815 + 1.232 × RER) × VO_2/lean mass.

Electron microscopy

BAT was cut into 1-mm^3 fragments, washed in fresh 0.1 M phosphate buffer (pH 7.4), and fixed in 2.5% glutaraldehyde in the same buffer at RT for 4 h. After three times of wash in fresh 0.1 M phosphate buffer (pH 7.4) for 10 min, tissues were fixed in 1% OsO_4 for 1 h at RT and washed three times in 0.1 M phosphate buffer for 10 min. Tissues were embedded in Epon (Sigma-Aldrich, 45,345), according to standard techniques, after dehydration with ethyl alcohol and propylene oxide. Ultrathin sections (60 nM) were cut from the blocks. The sections were collected and stained with uranyl acetate, followed by lead citrate, and then observed using a JEM 1400 transmission electron microscope (JEOL Ltd).

Cold tolerance test

Solitary caged mice were kept at 4°C for 6 h, and a control experiment was carried out at RT. Afterward, rectal temperatures were measured using a microprobe thermometer (Physitemp).

Western blot analysis

BAT and primary brown adipocytes were lysed using tissue extraction reagent I (Invitrogen, FNN0071) or NP40 cell lysis buffer (Invitrogen, FNN0021) containing protease/phosphatase inhibitor cocktail (Roche, 04693132001) and 1 mM phenylmethylsulfonyl fluoride (Sigma-Aldrich, P7626). Soluble proteins (10 μg per lane) were separated on a 12% SDS polyacrylamide gel and blotted on a nitrocellulose membrane (GE Healthcare, 1060004). Membranes were incubated with primary antibody at 4°C overnight, and horseradish peroxidase-conjugated secondary antibody at RT for 1 h in 5% skim

milk (Carl Roth, T145.2) with TBST, visualized using an chemiluminescence detection system (NLRP3: GeneDepot, W3680-010; CASP1: Biomax, BWD0100; UCP1 and ACTB: Biomax, BWP0200), and exposed to film (Agfa, CP-BU NEW). To determine the available linear range of western blots, the exposure time was collected in every experiment.

Anti-UCP1 (1:10,000 dilution) antibody was purchased from Abcam (ab10983). Anti-NLRP3 (1:1,000 dilution) and anti-CASP1 (1:2,000 dilution) antibodies were purchased from Adipogen (AG-20B-0014-C100, AG-20B-0042-C100). Anti-ACTB (1:20,000 dilution) antibody was purchased from Sigma-Aldrich (A5441). The signal intensities of protein bands were quantified with the ImageJ software (NIH) and normalized using the intensity of the loading control ACTB.

Real-time polymerase chain reaction (PCR) analysis

Total RNA (2 μg) was reverse-transcribed using RevertAid First Strand cDNA Synthesis Kit (Thermo Scientific, K1622). *Tbp* was used as internal control. The primers were designed on the basis of nucleotide sequences in the GenBank database (Table S2). The relative amounts of the mRNAs were calculated using the relative *Ct* method (PerkinElmer Wallace).

Measurement of plasma metabolic parameters

Plasma glucose concentration was measured using a glucose analyzer (Yellow Springs, YSI 2300). Plasma INS was determined via radioimmunoassay (Linco Research, EZRMI-13 K). Plasma free fatty acid (FFA) concentration was assayed using an enzymatic assay kit (Wako Chemical, C1057).

Measurement of INS (insulin) sensitivity

Following an overnight fast, a 2-h hyperinsulinemic-euglycemic clamp study was carried out with a primed-continuous infusion of human INS (Humulin, Eli Lilly) at a rate of 5 mU/kg/min with 150 mU/kg body weight priming. Blood samples (20 μl) were collected at 20 min intervals for immediate measurement of plasma glucose concentration, and 20% glucose was infused at variable rates to maintain plasma glucose at the basal concentration (~120 mg/dl) [49]. The ITT was performed in mice fasted for 5 h in the morning. Mice were intraperitoneally injected with 0.75 mU/kg of regular human INS. Blood was collected before injection and at 15, 30, 60, 90, and 120 min after injection for the measurement of blood glucose level. The glucose disappearance rate for the ITT (*k*ITT) was calculated using the formula *k*ITT (%/min) = 0.693/$t½$, where $t½$ is derived from the slope of the plasma glucose concentration from 0 to 15 min after INS injection [50].

Immunohistochemistry of UCP1

UCP1 immunostaining was calibrated on a Benchmark XT staining module (Ventana Medical Systems). The slides were warmed to 60°C for 1 h and then processed with a fully automated protocol. After the sections were dewaxed and rehydrated, CC1 (Ventana Medical Systems) pre-treatment was carried out for 60 min for antigen retrieval. Tissue sections were stained with rabbit polyclonal anti-UCP1 antibody (1:500; Abcam, ab10983) at 37°C for 36 min, and then with secondary Discovery UltraMap anti-rabbit horseradish peroxidase antibody (Ventana Medical Systems) at 37°C for 36 min. Detection was performed using the UltraView DAB (3,3′-diaminobenzidine) detection kit (Ventana Medical Systems). Counterstaining was conducted for 4 min using hematoxylin (Ventana Medical Systems). After completion of the automated staining protocol, the slides were dehydrated in 90% ethanol for 1 min, followed by 100% ethanol for 1 min. Before cover-slipping, the sections were cleared in xylene for 1 min and mounted with a synthetic mountant (Thermo Fisher Scientific). The samples were visualized using a BX53 upright microscope (Olympus) and CellSens software (Olympus).

Isolation of BAPs and culture

BAPs were isolated from interscapular BAT, as previously described [25]. Cells were grown to 70%–80% confluence before passaging every week.

Measurement of mitochondrial ROS generation

Mitochondria-specific ROS generation was monitored by fluorescence-activated cell sorting analysis using the MitoSox Red fluorescent dye (Molecular Probes, ENZ-51011).

Differentiation into brown adipocytes

Confluent cultures of BAPs were exposed to α-MEM (Welgene; LM008-01) differentiation medium containing dexamethasone (1 μM; Sigma-Aldrich, D4902), INS/insulin (850 nM; Sigma-Aldrich, I6634), isobutylmethylxanthine (0.5 mM; Sigma-Aldrich, 5879), indomethacin (125 μM; Sigma-Aldrich, I7378), rosiglitazone (1 μM; Cayman Chemical, 71740), T3 (1 nM; Sigma-Aldrich, T2877), and 10% FBS (Gibco Life Technologies, 16000044). Three days after differentiation, the cells were maintained in media containing INS (850 nM), rosiglitazone (1 μM), T3 (1 nM), and 10% FBS until they were ready for collection.

Phase-contrast microscopy

Cell images were acquired using an image capture system, consisting of an IX70 inverted microscope (Olympus).

Oil Red O staining

Differentiated brown adipocytes were fixed with 10% formaldehyde for 20 min. After washing with PBS, the cells were stained with Oil Red O solution (Sigma-Aldrich, O1516) for 30 min. The slides were then washed several times with water, and excess water was evaporated by heating the stained cultures to approximately 32°C.

Dual-energy X-ray absorptiometry (DEXA)

Body composition was determined using the INSIGHT VET DXA (Osteosys) at 16 weeks with or without HFD exposure.

To ensure good immobilization, mice were anesthetized with an intraperitoneal injection of 40 mg/kg ketamine and 0.8 mg/kg medetomidine. The weights of lean tissue and fat tissue were provided by the scanner, as previously reported [51].

Image analysis

The images of *in vitro* confocal imaging, *in vivo* H&E cross-sections, and EM images were quantified using ImageJ (NIH). Cell size was averaged from 10 representative images per H&E-stained sections or EM images from four mice. For measurement of *in vitro* lipid droplet area, 10 random images were examined per sample with four samples per condition.

Detection of mitophagy using mt-Keima

For mitophagy evaluation [29], mt-Keima lentivirus-infected BAPs were treated with 10 μM carbonyl cyanide *m*-chlorophenylhydrazone (Sigma-Aldrich, C2759) and 2 μM oligomycin (Sigma-Aldrich, O4876), or serum-free media, and analyzed using a confocal microscope (LSM780, Carl Zeiss). Images of fluorescent protein mt-Keima (emission at 588–633 nm) were taken at excitation wavelengths of 458 and 561 nm, and the GFP-fused protein (emission at 510 nm) was imaged using a 488 nm excitation filter.

Inflammasome activation

BAPs (1.0×10^6 cells per well) or BMDMs (1.0×10^6 cells per well) from WT or *pink1* KO mice were plated in 12-well plates and then primed for 4 h with 100 ng/ml LPS (Sigma-Aldrich, L6529) in RPMI 1640 medium (Welgene, LM011-01) containing 10% FBS and antibiotics. For the last 30 min, the medium was replaced with RPMI 1640 medium supplemented with 5 mM ATP (Sigma-Aldrich, A6419). IL1B in the media was quantified using an ELISA kit (R&D Systems, DY-401).

Isolation of BMDMs

Bone marrow cells were flushed from the femurs and tibias of mice and then depleted of RBCs using RBC lysis buffer (Sigma-Aldrich, R7757). The cells were then cultured in Dulbecco's modified Eagle's medium (DMEM; Welgene, LM001-05) supplemented with 10% FBS and 20 ng/ml murine CSF1 (Peprotech, 315–02). Non-adherent cells were carefully removed, and fresh medium was added every 2 d. On day 6, the cells were collected for experiments [52].

Plasmids and lentiviruses

To produce *GFP–Prkn*, – *Nlrp3*, – *Pink1*, and mt-Keima lentiviruses, GFP–*Prkn*, – *Nlrp3*, – *Pink1*, and mt-Keima (Addgene, 72342, Richard Youle) were subcloned into the pCDH-MCS lentiviral vector (System Biosciences, CD513B-1), and the plasmids were transfected in Lenti-X 293T cells (Clontech, 632180) along with packaging plasmids pMDLg/pRRE (Addgene, 12251, Didier Trono) and pRSV-Rev (Addgene, 12253, Didier Trono) and envelope plasmid pCMV-VSV-G (Addgene, 8454, Bob Weinberg) using Lipofectamine 3000 (Invitrogen, L30000015).

ChIP assay

The ChIP assay was performed with a ChIP-IT express kit (Active Motif, 53014). Undifferentiated BAPs (1×10^7) or differentiated BAPs (1×10^6) from WT or *pink1* KO mice were fixed with 1% formaldehyde at RT for 15 min to allow cross-linking of DNA with proteins, and glycine solution (final concentration of 0.125 M) was added to stop the cross-linking reaction. The fixed BAPs were lysed using a Dounce homogenizer to induce nuclei release. After sonication, the chromatins were immunoprecipitated overnight at 4°C with 2 μg anti-NLRP3 (AdipoGen Life Sciences, AG-20B-0014) and protein G magnetic beads. The chromatins were then washed and eluted from the protein G magnetic beads using buffers supplied with the kit DNA was purified using a ChIP DNA Clean and Concentration kit (Zymo Research, D5201) and analyzed by quantitative PCR (**Table S2**).

Statistical analysis

Data are expressed as mean ± standard error of the mean (SEM). Unpaired two-tailed Student's *t*-tests were used to compare variables between the two groups. One-way ANOVA was used to compare multiple groups. For the comparison of multiple measurements made at different time points, one-way repeated-measures ANOVA was used. Bonferroni correction was applied for post hoc analysis of the multiple comparisons. All statistical tests were conducted according to two-sided sample sizes and were determined on the basis of previous experiments using similar methods. For all experiments, all stated replicates are biological replicates. Statistical analysis and graphing were performed using IBM SPSS Statistics version 22.0 (IBM Corp.) or GraphPad Prism 7 (GraphPad Software).

Acknowledgments

We thank the Mary Lyon Centre at the MRC Harwell Institute, Oxfordshire, UK, for their donation of *pink1* KO mice. We also thank the Confocal Microscopy Core Facility at the Convergence Medicine Research Center (CREDIT), Asan Medical Center, for support and instrumentation, and Dr. Joon Seo Lim from the Scientific Publications Team at Asan Medical Center for his editorial assistance in preparing this manuscript. We thank Hwa Jung Kim from the University of Ulsan College of Medicine for assistance with statistical analysis.

Disclosure statement

No potential conflict of interest was reported by the authors.

Funding

This study was supported by grants from the following organizations: the National Research Foundation of Korea (NRF), funded by the Ministry of Education, Science, and Technology, Korea [NRF 2009-0091988, 2017R1E1A1A01073206: K.-U.L., 2017R1E1A1A01074207: E.H.K., 2013R1A1A2060600: J.Y.Y., 2013R1A1A2060750: M.S.K.]; the National Institutes of Health, USA [R01DK114356: S.M.H.]; the American Diabetes Association, USA [1-18-IBS-105: S.M.H.].

ORCID

In-Jeoung Baek http://orcid.org/0000-0002-0641-7208
Jung Jin Hwang http://orcid.org/0000-0003-0912-1055

Seung Eun Lee http://orcid.org/0000-0003-1463-6133
David A. Bader http://orcid.org/0000-0003-0514-7346
Chul-Ho Lee http://orcid.org/0000-0002-6996-5746
Eun-Gyoung Hong http://orcid.org/0000-0003-3390-5706
Un Jung Kang http://orcid.org/0000-0002-5970-6839

References

[1] Cypess AM, Lehman S, Williams G, et al. Identification and importance of brown adipose tissue in adult humans. N Engl J Med. 2009;360(15):1509–1517. . PMID:19357406
[2] Peirce V, Carobbio S, Vidal-Puig A. The different shades of fat. Nature. 2014;510(7503):76–83. . PMID:24899307
[3] Lowell BB, Spiegelman BM. Towards a molecular understanding of adaptive thermogenesis. Nature. 2000;404(6778):652–660. . PMID:10766252
[4] Cypess AM, White AP, Vernochet C, et al. Anatomical localization, gene expression profiling and functional characterization of adult human neck brown fat. Nat Med. 2013;19(5):635–639. . PMID:23603815
[5] Harms M, Seale P. Brown and beige fat: development, function and therapeutic potential. Nat Med. 2013;19(10):1252–1263. . PMID:24100998
[6] Kajimura S, Seale P, Spiegelman BM. Transcriptional control of brown fat development. Cell Metab. 2010;11(4):257–262. . PMID:20374957
[7] Zhang Y, Goldman S, Baerga R, et al. Adipose-specific deletion of autophagy-related gene 7 (atg7) in mice reveals a role in adipogenesis. Proc Natl Acad Sci U S A. 2009;106(47):19860–19865. . PMID:19910529
[8] Singh R, Xiang Y, Wang Y, et al. Autophagy regulates adipose mass and differentiation in mice. J Clin Invest. 2009;119(11):3329–3339. . PMID:19855132
[9] Altshuler-Keylin S, Shinoda K, Hasegawa Y, et al. Beige adipocyte maintenance is regulated by autophagy-induced mitochondrial clearance. Cell Metab. 2016;24(3):402–419. . PMID:27568548
[10] Green DR, Galluzzi L, Kroemer G. Mitochondria and the autophagy-inflammation-cell death axis in organismal aging. Science. 2011;333(6046):1109–1112. . PMID:21868666
[11] Youle RJ, Narendra DP. Mechanisms of mitophagy. Nat Rev Mol Cell Biol. 2011;12(1):9–14. . PMID:21179058
[12] Jang JY, Blum A, Liu J, et al. The role of mitochondria in aging. J Clin Invest. 2018;128(9):3662–3670. . PMID:30059016
[13] Franks PW, Scheele C, Loos RJ, et al. Genomic variants at the PINK1 locus are associated with transcript abundance and plasma nonesterified fatty acid concentrations in European whites. Faseb J. 2008;22(9):3135–3145. . PMID:18495756
[14] Schroder K, Zhou R, Tschopp J. The NLRP3 inflammasome: a sensor for metabolic danger? Science. 2010;327(5963):296–300. . PMID:20075245
[15] Strowig T, Henao-Mejia J, Elinav E, et al. Inflammasomes in health and disease. Nature. 2012;481(7381):278–286. . PMID:22258606
[16] Davis BK, Wen H, Ting JP. The inflammasome NLRs in immunity, inflammation, and associated diseases. Annu Rev Immunol. 2011;29707–29735. DOI:10.1146/annurev-immunol-031210-101405. PMID:21219188
[17] Goldberg EL, Dixit VD. Drivers of age-related inflammation and strategies for healthspan extension. Immunol Rev. 2015;265(1):63–74. . PMID:25879284
[18] Nakahira K, Haspel JA, Rathinam VA, et al. Autophagy proteins regulate innate immune responses by inhibiting the release of mitochondrial DNA mediated by the NALP3 inflammasome. Nat Immunol. 2011;12(3):222–230. . PMID:21151103
[19] Zhou R, Yazdi AS, Menu P, et al. A role for mitochondria in NLRP3 inflammasome activation. Nature. 2011;469(7329):221–225. . PMID:21124315
[20] Bruchard M, Rebe C, Derangere V, et al. The receptor NLRP3 is a transcriptional regulator of TH2 differentiation. Nat Immunol. 2015;16(8):859–870. . PMID:26098997
[21] Gautier CA, Kitada T, Shen J. Loss of PINK1 causes mitochondrial functional defects and increased sensitivity to oxidative stress. Proc Natl Acad Sci U S A. 2008;105(32):11364–11369. . PMID:18687901
[22] Shimizu I, Aprahamian T, Kikuchi R, et al. Vascular rarefaction mediates whitening of brown fat in obesity. J Clin Invest. 2014;124(5):2099–2112. . PMID:24713652
[23] Feldmann HM, Golozoubova V, Cannon B, et al. UCP1 ablation induces obesity and abolishes diet-induced thermogenesis in mice exempt from thermal stress by living at thermoneutrality. Cell Metab. 2009;9(2):203–209. . PMID:19187776
[24] Zhu J, Wang KZ, Chu CT. After the banquet: mitochondrial biogenesis, mitophagy, and cell survival. Autophagy. 2013;9(11):1663–1676. . PMID:23787782
[25] Cannon B, Nedergaard J. Cultures of adipose precursor cells from brown adipose tissue and of clonal brown-adipocyte-like cell lines. Methods Mol Biol. 2001;155213–155224. DOI:10.1385/1-59259-231-7:213. PMID:11293074
[26] Oh J, Lee YD, Wagers AJ. Stem cell aging: mechanisms, regulators and therapeutic opportunities. Nat Med. 2014;20(8):870–880. . PMID:25100532
[27] Graja A, Schulz TJ. Mechanisms of aging-related impairment of brown adipocyte development and function. Gerontology. 2015;61(3):211–217. . PMID:25531079
[28] Ferree AW, Trudeau K, Zik E, et al. MitoTimer probe reveals the impact of autophagy, fusion, and motility on subcellular distribution of young and old mitochondrial protein and on relative mitochondrial protein age. Autophagy. 2013;9(11):1887–1896. . PMID:24149000
[29] Sun N, Malide D, Liu J, et al. A fluorescence-based imaging method to measure in vitro and in vivo mitophagy using mt-Keima. Nat Protoc. 2017;12(8):1576–1587. . PMID:28703790
[30] Stienstra R, Joosten LA, Koenen T, et al. The inflammasome-mediated caspase-1 activation controls adipocyte differentiation and insulin sensitivity. Cell Metab. 2010;12(6):593–605. . PMID:21109192
[31] Wree A, Eguchi A, McGeough MD, et al. NLRP3 inflammasome activation results in hepatocyte pyroptosis, liver inflammation, and fibrosis in mice. Hepatology. 2014;59(3):898–910. . PMID:23813842
[32] Shahzad K, Bock F, Dong W, et al. Nlrp3-inflammasome activation in non-myeloid-derived cells aggravates diabetic nephropathy. Kidney Int. 2015;87(1):74–84. . PMID:25075770
[33] Linhart HG, Ishimura-Oka K, DeMayo F, et al. C/EBPalpha is required for differentiation of white, but not brown, adipose tissue. Proc Natl Acad Sci U S A. 2001;98(22):12532–12537. . PMID:11606718
[34] Yang J, Croniger CM, Lekstrom-Himes J, et al. Metabolic response of mice to a postnatal ablation of CCAAT/enhancer--binding protein alpha. J Biol Chem. 2005;280(46):38689–38699. . PMID:16166091
[35] Rosen ED, Hsu CH, Wang X, et al. C/EBPalpha induces adipogenesis through PPARgamma: a unified pathway. Genes Dev. 2002;16(1):22–26. . PMID:11782441
[36] Elberg G, Gimble JM, Tsai SY. Modulation of the murine peroxisome proliferator-activated receptor gamma 2 promoter activity by CCAAT/enhancer-binding proteins. J Biol Chem. 2000;275(36):27815–27822. . PMID:10862621
[37] Wu Z, Rosen ED, Brun R, et al. Cross-regulation of C/EBP alpha and PPAR gamma controls the transcriptional pathway of adipogenesis and insulin sensitivity. Mol Cell. 1999;3(2):151–158. . PMID:10078198
[38] Qiao L, Maclean PS, Schaack J, et al. C/EBPalpha regulates human adiponectin gene transcription through an intronic enhancer. Diabetes. 2005;54(6):1744–1754. . PMID:15919796

[39] Sliter DA, Martinez J, Hao L, et al. Parkin and PINK1 mitigate STING-induced inflammation. Nature. 2018;561(7722):258–262. . PMID:30135585
[40] Lu Y, Fujioka H, Joshi D, et al. Mitophagy is required for brown adipose tissue mitochondrial homeostasis during cold challenge. Sci Rep. 2018;8(1):8251. . PMID:29844467
[41] Mottillo EP, Desjardins EM, Crane JD, et al. Lack of adipocyte AMPK exacerbates insulin resistance and hepatic steatosis through brown and beige adipose tissue function. Cell Metab. 2016;24(1):118–129. . PMID:27411013
[42] Lu X, Altshuler-Keylin S, Wang Q, et al. Mitophagy controls beige adipocyte maintenance through a Parkin-dependent and UCP1-independent mechanism. Sci Signal. 2018;11(527):eaap8526. . PMID:29692364
[43] Wang W, Seale P. Control of brown and beige fat development. Nat Rev Mol Cell Biol. 2016;17(11):691–702. . PMID:27552974
[44] Swanson KV, Deng M, Ting JP. The NLRP3 inflammasome: molecular activation and regulation to therapeutics. Nat Rev Immunol. 2019;19(8):477–489. . PMID:31036962
[45] Townsend KL, Tseng YH. Brown fat fuel utilization and thermogenesis. Trends Endocrinol Metab. 2014;25(4):168–177. . PMID:24389130
[46] Petersen MC, Shulman GI. Mechanisms of insulin action and insulin resistance. Physiol Rev. 2018;98(4):2133–2223. . PMID:30067154
[47] Xiong H, Wang D, Chen L, et al. Parkin, PINK1, and DJ-1 form a ubiquitin E3 ligase complex promoting unfolded protein degradation. J Clin Invest. 2009;119(3):650–660. . PMID:19229105
[48] Sung YH, Baek IJ, Kim DH, et al. Knockout mice created by TALEN-mediated gene targeting. Nat Biotechnol. 2013;31(1):23–24. PMID:23302927
[49] Hong EG, Ko HJ, Cho YR, et al. Interleukin-10 prevents diet-induced insulin resistance by attenuating macrophage and cytokine response in skeletal muscle. Diabetes. 2009;58(11):2525–2535. . PMID:19690064
[50] Masi LN, Martins AR, Crisma AR, et al. Combination of a high-fat diet with sweetened condensed milk exacerbates inflammation and insulin resistance induced by each separately in mice. Sci Rep. 2017;7(1):3937. . PMID:28638152
[51] Gargiulo S, Gramanzini M, Megna R, et al. Evaluation of growth patterns and body composition in C57Bl/6J mice using dual energy X-ray absorptiometry. Biomed Res Int. 2014:2014253067. DOI:10.1155/2014/253067. PMID:25110666
[52] Mao K, Chen S, Chen M, et al. Nitric oxide suppresses NLRP3 inflammasome activation and protects against LPS-induced septic shock. Cell Res. 2013;23(2):201–212. . PMID:23318584